On the effects of different strategies in modelling balloon-expandable stenting by means of finite element method

Francesca Gervaso*, Claudio Capelli, Lorenza Petrini, Simone Lattanzio,
Luca Di Virgilio, Francesco Migliavacca

Laboratory of Biological Structure Mechanics, Department of Structural Engineering, Politecnico di Milano, Piazza L. da Vinci 32, 20133 Milan, Italy

Abstract

In recent years, computational structural analyses have emerged as important tools to investigate the mechanical response of stent placement into arterial walls. Although most coronary stents are expanded by inflating a polymeric balloon, realistic computational balloon models have been introduced only recently. In the present study, the finite element method is applied to simulate three different approaches to evaluate stent-free expansion and stent expansion inside an artery. Three different stent expansion modelling techniques were analysed by: (i) imposing a uniform pressure on the stent internal surface, (ii) a rigid cylindrical surface expanded with displacement control and (iii) modelling a polymeric deformable balloon. The computational results showed differences in the free and confined-stent expansions due to different expansion techniques. The modelling technique of the balloon seems essential to estimate the level of injury caused on arterial walls during stent expansion.

1. Introduction

Endovascular stents are medical devices inserted percutaneously into a stenotic artery to allow blood perfusion to the downstream tissues. Despite the recent advantages brought by the new generation devices such as drug-eluting stents, some critical issues still remain regarding the efficacy of such devices (Serruys and Kukreja, 2006). Restenosis, i.e. the re-narrowing of the artery after its treatment with angioplasty or stenting, is the most common occurrence after these procedures, which usually occurs a few months after the initial procedure (Serruys et al., 1998). Many factors have been found to influence the degree of restenosis, such as the degree of damaged endothelial cells and the depth of the injury (Schwartz et al., 1992; Kornowski et al., 1998), the plaque composition and shape, the type of stent expansion (self- or balloon expandable; Harnek et al., 2002; Morton et al., 2004), the design of the stent (Rogers and Edelman,

1995; Edelman and Rogers, 1998) and the local fluid dynamics (Wentzel et al., 2001). As the stent deployment inside an artery generates anomalous stresses and deformations in arterial walls, it is easy to imagine that it might have some influence on the later progression of in-stent restenosis. In recent years, computational structural analyses have emerged as an important tool to investigate the mechanical response to angioplasty and stent placement inside arterial walls (Lee et al., 1993; Oh et al., 1994; Rogers et al., 1999; Gourisankaran and Sharma, 2000; Auricchio et al., 2001; Holzapfel et al., 2002, 2005a; Prendergast et al., 2003; Migliavacca et al., 2004, 2005, 2007; Lally et al., 2005; Liang et al., 2005; De Beule et al., 2006; Bedoya et al., 2006; Hall and Kasper, 2006; Ballyk, 2006; Wang et al., 2006; Takashima et al., 2007; Wu et al., 2007).

Most of the available stents use a folded polymeric balloon that is inflated on insertion. The effect of balloon inflation on arterial walls is not insignificant, since as the balloon starts to open from its heads, it stresses the surrounding vascular tissue. In the recent literature, the stent has been expanded by imposing pressure to the

*Corresponding author. Tel.: +39 02 2399 4283; fax: +39 02 2399 4286.
E-mail address: francesca.gervaso@polimi.it (F. Gervaso).

internal stent struts (Dumoulin and Cochelin, 2000; Migliavacca et al., 2002, 2005; Holzapfel et al., 2005a; De Beule et al., 2006) or by enlarging a rigid cylinder inside the stent in displacement control (Hall and Kasper, 2006; Takashima et al., 2007; Wu et al., 2007). In other studies, the balloon is modelled as a silicon cylinder using either a linear elastic (Wang et al., 2006), a bilinear hyperelastic material capable of modelling the unfolding phase of the balloon (Liang et al., 2005; Raamachandran and Jayaven-kateshwaran, 2007) or a trifolded elastic cylinder (De Beule et al., 2007). Moreover, based on our knowledge of balloon modelling, a balloon accounting for the presence of heads has been proposed only recently by Gasser and Holzapfel (2007), and Ju et al. (2008). The former showed a detailed stress analysis of the arterial tissue based on a balloon/artery contact and proposed a finite element simulation of a Gruentzig-type balloon catheter; the latter limited their analyses to the interaction of the stent and the balloon. However, the effects of different expansion procedures on the stent and on the arterial wall have not been carefully analysed.

The objective of this study is to present three different modelling solutions (namely the load, the displacement control conditions and the modelling of balloon expansion) that could be adopted to study stent-free expansion and stent expansion inside an artery. Indeed, it is important to understand not only the mechanical response of the stent in the design phase, but also the arterial stress status caused by the device. Advantages and disadvantages of the different modelling strategies are presented and discussed.

2. Materials and methods

Three finite element simulations of stent expansion were performed with the following loading conditions: (i) a uniform pressure imposed on its internal surface, (ii) a rigid cylindrical surface expanded with displacement control and (iii) a polymeric deformable balloon previously deflated. Two sets of simulations were run; in one of them, the stent was *freely* expanded; in the other, the stent expansion was *confined* into a model of artery to evaluate the influence of the modelling technique on stress and deformation states of the arterial wall.

2.1. Geometry and meshes

The stent used in this study resembles the coronary Cordis BX-Velocity (Johnson & Johnson, Interventional System, Warren, NJ, USA) with a nominal diameter of 3.5 mm. This stent is composed of four tubular-like rings, the struts, connected by bridging members, the links (Fig. 1(a)). The stent geometry was created using Rhinoceros 3.0 Evaluation CAD program (McNeel & Associates, Indianapolis, IN, USA), after an acquisition of the Cordis dimensions by the use of a Nikon SMZ800 stereo microscope (Nikon Corporation, Tokyo, Japan). The stent length was 8.36 mm, the inner diameter was 1.2 mm (which was assumed to be the value prior to crimping) and the thickness was 0.14 mm. A mesh of 49775 3D 8-node cubic element was generated (inset of Fig. 1(top)).

The balloon was designed with a nominal diameter of 3.2 mm and a length of 12 mm. The mesh consisted of 4080 3D 4-node membrane elements and 96 3D 3-node membrane elements (thickness = 0.05 mm) in order to obtain the balloon heads. To obtain the initial deflated configuration of the balloon, a preliminary analysis was run, in which a negative pressure of 0.01 MPa was applied to its inner surface (Fig. 1
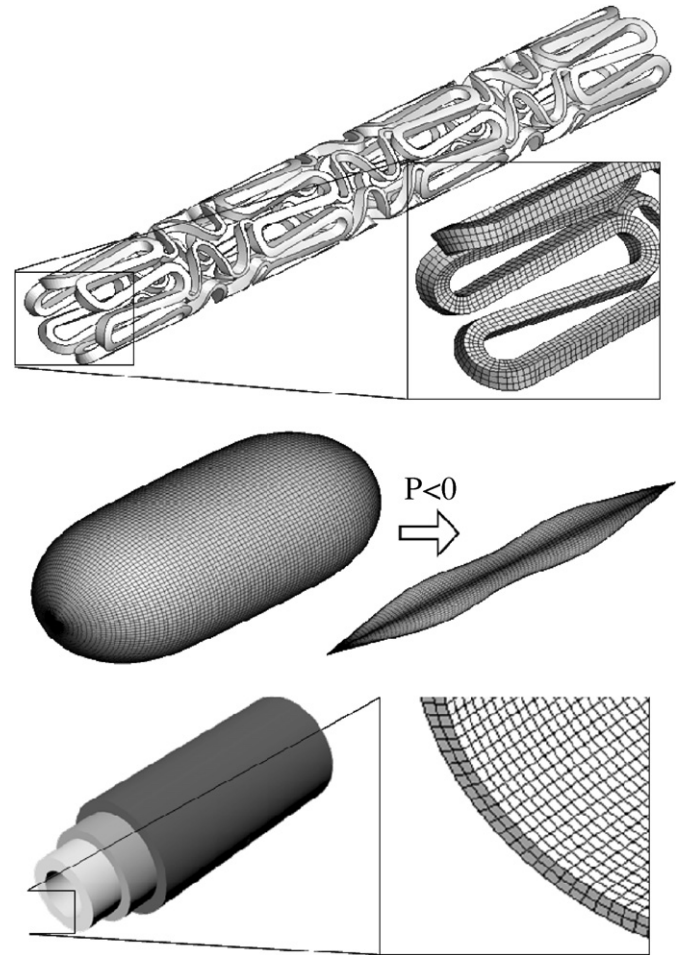

Fig. 1. (top) Stent design and mesh. (middle) The polymeric balloon before (left) and after (right) the deflation. (bottom) The three-layer coronary artery and its discretization.

middle). Once deflated, the folded balloon can easily be inserted inside the stent.

The coronary artery was modelled as a hollow cylinder with an internal radius of 1.25 mm, a thickness of 0.5 mm and a length of 10 mm. The artery was then partitioned into three layers of equal thickness, representing the intima, the media and the adventitia (Fig. 1bottom). A bond of perfect adhesion exists between each pair of vessel layers. The artery was meshed with 87750 3D 8-node cubic solid elements (inset of Fig. 1 bottom).

In order to verify the goodness of the mesh density used in the analyses, a mesh dependency study was run, expanding either the stent or the artery to a diameter of 3 mm. The stent mesh density was increased from 9969 to 19,937 elements for unit. The percentage difference of Von Mises stresses between the finest and selected meshes was 0.3%. The artery mesh density was increased from 7050 to 280,098 elements. No notable difference in Von Mises stresses between the finest and the selected meshes was observed.

2.2. Constitutive models

The stent was assumed to be made of 316L stainless steel. The steel was modelled as a homogeneous, isotropic, elasto-plastic material through a Von Mises–Hill plasticity model with a Young modulus of 193 GPa, a Poisson coefficient of 0.3 and a yield stress of 205 MPa.

Table 1
Material coefficients of the strain energy density function for intima, media and adventitia layers

	C_{10}	C_{20}	C_{30}	C_{40}	C_{50}	C_{60}
Intima	6.79E−03	0.54	−1.11	10.65	−7.27	1.63
Media	6.52E−03	4.89E−02	9.26E−03	0.76	−0.43	8.69E−02
Adventitia	8.27E−03	1.20E−02	0.52	−5.63	21.44	0.00

A semi-compliant balloon was modelled with an isotropic, linear-elastic material, with a Young modulus of 900 MPa and a Poisson coefficient of 0.3.

The work of Holzapfel et al. (2005b) was adopted to describe the mechanical behaviour of the coronary artery. In particular, a hyperelastic isotropic constitutive model consistent with the mean values of their experimental results in the circumferential direction was used. The constitutive law was based on a reduced polynomial strain energy density function, U, of sixth order:

$$U = C_{10}(\bar{I}_1 - 3) + C_{20}(\bar{I}_1 - 3)^2 + C_{30}(\bar{I}_1 - 3)^3$$
$$+ C_{40}(\bar{I}_1 - 3)^4 + C_{50}(\bar{I}_1 - 3)^5 + C_{60}(\bar{I}_1 - 3)^6 \quad (1)$$

where $\bar{I}_1$ is the first invariant of the Cauchy–Green tensor:

$$\bar{I}_1 = \bar{\lambda}_1^2 + \bar{\lambda}_2^2 + \bar{\lambda}_3^2 \quad (2)$$

with $\bar{\lambda}_i = J^{-1/3}\lambda_i$, where λ_i are the principal stretches and J is the total volume ratio. Table 1 reports the values of the coefficients for each layer.

2.3. Boundary conditions and simulations

Two sets of three simulations each were performed; in one of them, the stent was freely expanded, while in the other, the stent was expanded into the model of the artery. The analyses were performed using the commercial code ABAQUS/Explicit v. 6.4. The large-deformation theory was used.

2.3.1. Free-expansion simulations
Three models, corresponding to three different methods of expansion, were created: the *free-LOAD*, the *free-CYLINDER* and the *free-BALLOON* models.

To avoid rigid movements of the stent, three nodes, located in the middle section of the stent and forming the vertices of an equilateral triangle, were constrained in the tangential and axial directions.

In the *free-LOAD* model, the stent was expanded by imposing a uniform pressure equal to 0.8 MPa on the internal surface of the stent.

In the *free-CYLINDER* model the stent was expanded by means of a cylinder. For this purpose, a linear elastic thin tube (Young modulus of 400,000 MPa, Poisson coefficient of 0.3) of radius 0.35 mm and length 18 mm was created and meshed with 6075 4-node shell elements. A radial displacement of 1.5 mm was imposed to the nodes of the cylinder. A frictionless contact between the internal stent surface and the external cylinder surface was defined to avoid surface penetration.

In the *free-BALLOON* model the stent was expanded by modelling a deflated balloon, as previously explained. To avoid potential rigid displacements, three nodes forming an equilateral triangle in the central cross-section of the balloon were constrained in axial and circumferential directions. In addition, the radial and tangential displacements of the two nodes located on the heads of the balloon were restricted to mimic the bond to the catheter. A pressure of 1.5 MPa was imposed on the internal surface of the deflated balloon. The internal stent and the external balloon surfaces were defined as two frictionless contact surfaces. Furthermore, since the stent deformations were significant, a self-contact was added onto the stent surfaces.

A quasi-static analysis was performed. The analysis was considered quasi-static when the kinetic energy of the deforming material did not exceed 5% of its internal energy throughout most of the process, as recommended by ABAQUS. This condition was obtained by setting the step time of the simulations to 3 s.

The results of the three stent expansion techniques were compared in terms of Von Mises stresses and deformed configurations. In addition, the foreshortening of the stent was evaluated for all the three models as $fs = (l_0 - l_f)/l_0$, where l_0 and l_f are the initial and the final stent length, respectively. Lastly, for the *free-BALLOON* model only, the dogboning was calculated as: $d_b = (d_e - d_c)/d_e$, where d_e and d_c are the external and the central diameter of the stent at the end of the expansion, respectively.

2.3.2. Confined-expansion simulations
The stent was expanded following the same methods illustrated for the three free expansions, confining it inside the coronary artery model. The three models are referred to as: the *confined-LOAD*, the *confined-CYLINDER* and the *confined-BALLOON* models.

To reduce the long computational time for this set of simulations, only a unit of the stent consisting of two struts (length = 3.68 mm) was modelled. A shorter balloon (inflated balloon length = 8 mm) was designed, conserving the same stent-length/balloon-length ratio of the previous free-expansion simulations.

Three nodes forming the vertices of an equilateral triangle located in the middle cross-section of the artery were constrained in the tangential and axial direction to avoid possible rigid movements. The artery could freely expand in the radial direction.

In all the models, a frictionless, exponential contact between the external surface of the stent and the internal surface of the artery was defined; a further contact was imposed between the internal surface of the stent and the external surface of the cylinder or the balloon, in the *confined-CYLYNDER* and *confined-BALLOON* models, respectively. Furthermore, as in the *free-BALLOON* model, a self-contact was added onto the stent surfaces.

Each simulation consisted of two steps: in the former, a pressure of 100 mmHg was imposed on the internal surface of the artery to mimic the physiological conditions; in the latter, the stent was expanded, each model by the technique previously described.

The main quantities of interest evaluated were the stresses (axial, radial and circumferential components) in the arterial wall.

3. Results

3.1. Free expansion

The deformed configurations of the stent at the beginning, the middle and the end of the stent expansion process are shown in Fig. 2 for the three models investigated. The stent expanded under load control conditions (*free-LOAD* model) presented a barrel-shape during all the expansion phases, while the stent opened by the cylinder (*free-CYLINDER* model) maintained its cylindrical shape according to the linear displacement imposed to the inner cylinder. Conversely, the *free-BALLOON* model started to open the stent from the heads, showing the well-known dogboning shape; as the pressure was increased, the central part of the structure also enlarged. It is also noticeable that once the balloon had reached its nominal diameter, further increases in pressure had no significant effect on its size. This finding is consistent with the hypothesis of the semi-compliant balloon used in reality. This behaviour is shown in the pressure vs. diameter diagram (Fig. 3), where the data supplied by the company are reported as well.
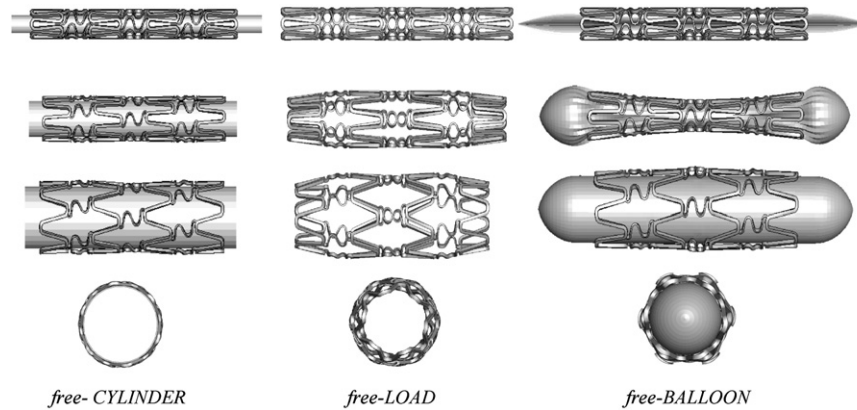
Fig. 2. Deformed shape of the three models at the initial (top), the midterm (middle) and the end (bottom) of the stenting procedure simulation.
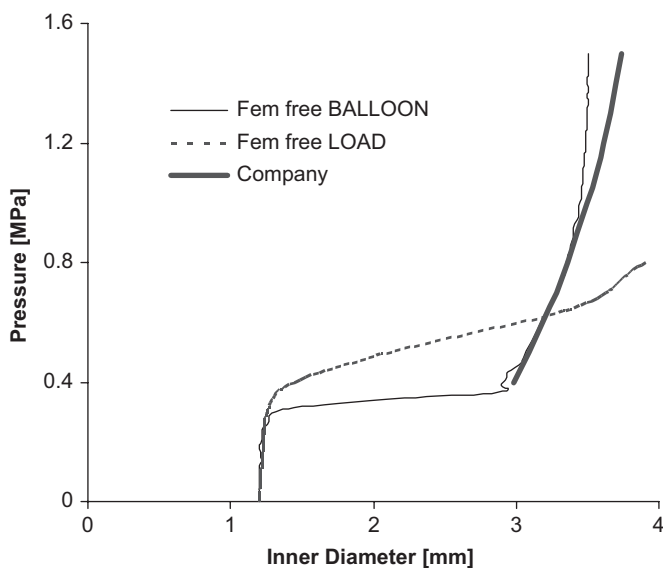

Fig. 3. Pressure–diameter curves of the *free-BALLOON* and *free-LOAD* models compared to the data available from the manufacturer.

Fig. 4 reports the maps of the Von Mises stresses for the *free-LOAD*, *free-CYLINDER* and *free-BALLOON* models. The maximum value (400 MPa) was localized in the most highly curved portion of the stent strut for all three models; material plasticization also occurred at the point of maximum stress, with a maximum equivalent plastic strain of 0.19 for each model. Detailed analysis of the stress distribution on the stent struts in the three models allowed calculation of the percentage of elements with a stress value included in a 100 MPa range (Table 2). The *free-CYLINDER* and *free-BALLOON* models presented a similar percentage of elements with the Von Mises stresses in the 100–200 and 200–300 MPa ranges, respectively. The *free-LOAD* model showed the most uniform stress distribution, having 45% of elements with a stress value between 200 and 300 MPa. At high stresses, the *free-BALLOON* stress distribution was notably lower than that of the other two models.

The foreshortening for the *free-LOAD*, *free-CYLINDER* and *free-BALLOON* models was about 6%, 10% and 9%, respectively. The maximum dogboning resulting from the *free-BALLOON* simulation was equal to 46%.

3.2. Confined expansion

In order to reduce the high computational cost of stent expansion simulation into the artery, a stent of two struts was used. To validate this assumption, the free expansion of this stent was analysed. The results showed that: (i) the maximum Von Mises stress was about 400 MPa and localized in the high curved part of the strut; (ii) the foreshortening was about 10% for all three models and (iii) the dogboning occurring in the balloon model was equal to 33.6%. The results are in good agreement with those of the longer stent, allowing the use of the short model.

As a consequence of vessel pressurization, the arterial diameter became equal to 3 mm and the maximum Von Mises stresses in the intima, media and adventitia were, respectively, 0.11, 0.012 and 0.009 MPa.

Fig. 5 depicts the radial, circumferential and axial stresses for the three models. The radial stresses are reported for three different times of the expansion. The *confined-CYLINDER* model causes a uniform imprint of the stent on the arterial wall during the stent expansion, while the circumferential stresses show a maximum value of 1.5 MPa inside the imprints left by the struts. In the *confined-LOAD* model, the radial stresses are concentrated next to the central section (0.8 MPa). The position of the maximal circumferential stresses (1.5 MPa) corresponds to the tracks left by the strut. The stent expanded by the *confined-BALLOON* model shows a particular behaviour during the transitory due to the dogboning effect. Specifically, two peaks of compressive radial stresses take place on the arterial wall due to the non-uniform expansion of the balloon (Fig. 5(a) arrows). Once the device is fully expanded, a further increase of the inflation pressure induces limited increments of stresses on the arterial wall, in accordance with the hypothesis of semi-compliant balloon. The presence of the balloon causes a more diffuse distribution of circumferential stresses as well as of radial
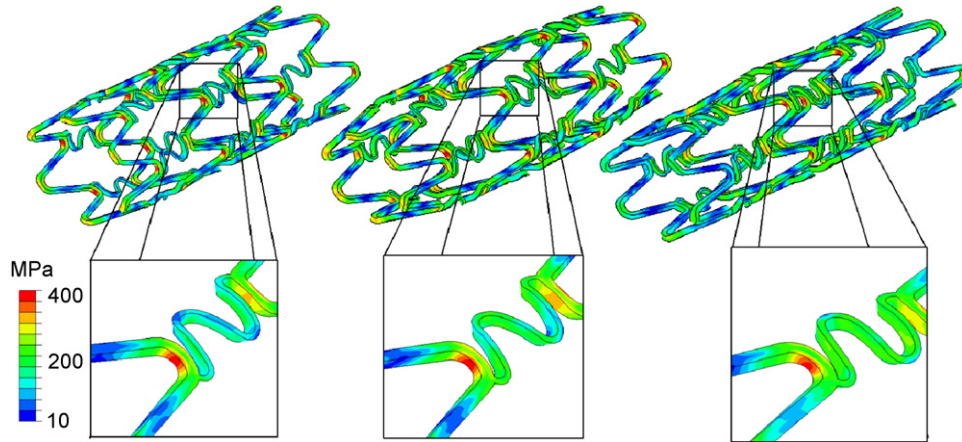
Fig. 4. The Von Mises stress maps for the *free-CYLINDER*, *free-LOAD* and *free-BALLOON* models.

Table 2
Von Mises stress distribution for each stent expansion model

Stress (MPa)	Element (%)		
	Free CYLINDER	*Free LOAD*	*Free BALLOON*
0–100	29.5	26.9	35.0
100–200	36.0	21.6	40.5
200–300	27.6	45.4	22.4
300–400	6.9	6.1	2.1

stresses. The analysis of axial stresses shows a similar distribution caused by the three models.

The different shapes obtained with different stent expansion techniques have different effects on stresses of the arterial wall.

4. Discussion

In this study, the effect of different stent expansion modelling techniques has been investigated by means of the finite element method. A model of a balloon commonly used to expand stents has also been developed to evaluate whether the balloon presence can be neglected in terms of effects on the stent and wall stresses. In particular, the threefolded balloon was simulated using a multi-folded model, including closed heads virtually linked to a catheter.

The developed models allowed analysis of important parameters that could play a role in the restenosis process, such as dogboning and foreshortening.

The results of the three free-expansion simulations presented similar values of the maximum Von Mises stress, localization of these stresses in the stent strut and foreshortening, showing that relating to these parameters, the three different techniques can be used interchangeably, even though the spatial stress distribution shows some differences, probably related to the different deformed shapes reached at the end of the expansion. Indeed, the deformed shapes, resulting from the three different

expansion procedures, showed significant differences. The dogboning phenomenon occurs only in the balloon expansion model.

The investigation of the results on the arterial wall confirms the differences caused by the three expansion methods. The analysis of radial stresses confirms the diversity in terms of distribution and values; the comparison of circumferential stress distribution shows the most significant difference, while the axial stresses are similar in each of the three cases, as expected.

Moreover, as deduced from the graph (Fig. 3), in the load model the increase in pressure means a direct increase of stresses on the arterial wall. Conversely, in the balloon model the transmission of the pressure increase to the vessel is very limited once the nominal diameter is reached. This result confirms that balloon modelling should be considered when simulating the stenting procedure.

4.1. Limitations

To reduce the very long computational time, only one unit of the stent was modelled in the confined expansions. However, the low difference between the short- and long-stent results in free expansion (a dogboning of 33.6% and 40%, respectively, was detected) suggests that even with the *confined-BALLOON* model the two stents should behave similarly.

The design of the balloon is not fully realistic from a geometrical point of view, but it is possible to assume that the functional behaviour is close to reality. Indeed, the contemporary presence of a multi-folded shape and of the heads of the balloon ensures a realistic semi-compliant expansion.

Intima, media and adventitia were modelled as isotropic materials; a more sophisticated material model—taking into account the different orientation of the collagen fibres of the vessel tissue and the presence of the atherosclerotic plaque—would be preferable.

Arterial prestretch was not included to reduce computation time for the simulations. Lastly, the artery was
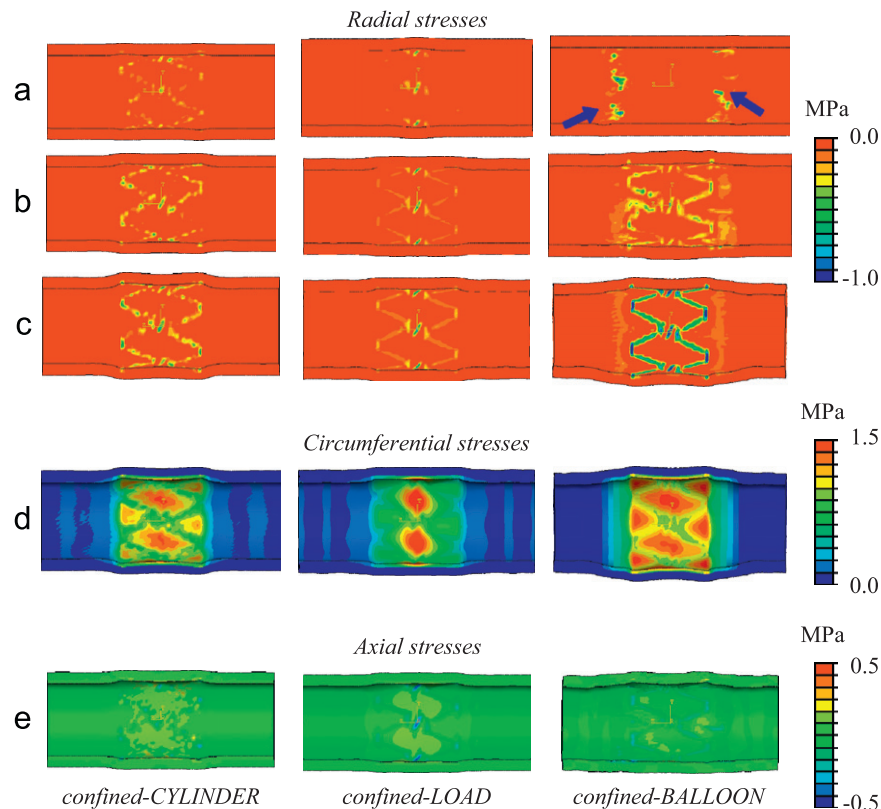
Fig. 5. Stress maps of the radial, circumferential and axial components for the three models. For the radial components, (a) and (b) refer to the beginning of the contact between stent and vessel wall and to the middle expansion, respectively; (c) refers to the ending instant of each simulation as (d) and (e) for the circumfrential and axial components.

modelled with a simplified geometry, whereas a realistic geometry obtained from clinical images could be used. Since the scope of this study was to compare three different techniques of stent expansion, this assumption has been judged acceptable.

In conclusion, this study presents a stenting model that operates in a realistic way and shows the differences occurring in free- and confined-stent expansion. The modelling of the balloon seems mandatory to estimate the level of injury caused on the arterial wall during stent expansion.

Conflict of interest

There are no conflicts of interest to declare by the authors.

Acknowledgements

References

Auricchio, F., Di Loreto, M., Sacco, E., 2001. Finite-element analysis of a stenotic revascularization through a stent insertion. Computer Methods in Biomechanics and Biomedical Engineering 4, 249–264.

Ballyk, P.D., 2006. Intramural stress increases exponentially with stent diameter: a stress threshold for neointimal hyperplasia. Journal of Vascular and Interventional Radiology 17, 1139–1145.

Bedoya, J., Meyer, C.A., Timmins, L.H., Moreno, M.R., Moore, J.E., 2006. Effects of stent design parameters on normal artery wall mechanics. Journal of Biomechanical Engineering 128, 757–765.

De Beule, M., Van Impe, R., Verhegghe, B., Segers, P., Verdonck, P., 2006. Finite element analysis and stent design: reduction of dogboning. Technology and Health Care 14, 233–241.

De Beule, M., Mortier, P., Carlier, S.G., Verhegghe, B., Van Impe, R., Verdonck, P., 2007. Realistic finite element-based stent design: the impact of balloon folding. Journal of Biomechanics, in press, doi:10.1016/j.jbiomech.2007.08.014.

Dumoulin, C., Cochelin, B., 2000. Mechanical behaviour modelling of balloon-expandable stents. Journal of Biomechanics 33, 1461–1470.

Edelman, E.R., Rogers, C., 1998. Pathobiologic responses to stenting. The American Journal of Cardiology 81, 4E–6E.

Gasser, T.C., Holzapfel, G.A., 2007. Finite element modeling of balloon angioplasty by considering overstretch of remnant non-diseased tissues in lesions. Computational Mechanics 40, 47–60.

Gourisankaran, V., Sharma, M.G., 2000. The finite element analysis of stresses in atherosclerotic arteries during balloon angioplasty. Critical Reviews in Biomedical Engineering 28, 47–51.

Hall, G.J., Kasper, E.P., 2006. Comparison of element technologies for modelling stent expansion. Journal of Biomechanical Engineering 128, 751–756.

Harnek, J., Zoucas, E., Stenram, U., Cwikiel, W., 2002. Insertion of self-expandable nitinol stents without previous balloon angioplasty reduces restenosis compared with PTA prior to stenting. Cardiovascular and Interventional Radiology 25, 430–436.

Holzapfel, G.A., Stadler, M., Schulze-Bauer, C.A., 2002. A layer-specific three-dimensional model for the simulation of balloon angioplasty using magnetic resonance imaging and mechanical testing. Annals of Biomedical Engineering 30, 753–767.

Holzapfel, G.A., Stadler, M., Gasser, T.C., 2005a. Changes in the mechanical environment of stenotic arteries during interaction with stents: computational assessment of parametric stent designs. Journal of Biomechanical Engineering 127, 166–180.

Holzapfel, G.A., Sommer, G., Gasser, C.T., Regitnig, P., 2005b. Determination of layer-specific mechanical properties of human coronary arteries with nonatherosclerotic intimal thickening and related constitutive modelling. American Journal of Physiology, Heart and Circulatory Physiology 289, H2048–H2058.

Ju, F., Xia, Z., Sasaki, K., 2008. On the finite element modelling of balloon-expandable stents. Journal of the Mechanical Behavior of Biomedical Materials 1, 86–95.

Kornowski, R., Hong, M.K., Tio, F.O., Bramwell, O., Wu, H., Leon, M.B., 1998. In-stent restenosis: contributions of inflammatory responses and arterial injury to neointimal hyperplasia. Journal of the American College of Cardiology 31, 224–230.

Lally, C., Dolan, F., Prendergast, P.J., 2005. Cardiovascular stent design and vessel stresses: a finite element analysis. Journal of Biomechanics 38, 1574–1581.

Lee, R.T., Loree, H.M., Cheng, G.C., Lieberman, E.H., Jaramillo, N., Schoen, F.J., 1993. Computational structural analysis based on intravascular ultrasound imaging before in vitro angioplasty: prediction of plaque fracture locations. Journal of the American College of Cardiology 21, 777–782.

Liang, D.K., Yang, D.Z., Qi, M., Wang, W.Q., 2005. Finite element analysis of the implantation of a balloon-expandable stent in a stenosed artery. International Journal of Cardiology 104, 314–318.

Migliavacca, F., Petrini, L., Colombo, M., Auricchio, F., Pietrabissa, R., 2002. Mechanical behavior of coronary stents investigated through the finite element method. Journal of Biomechanics 35, 803–811.

Migliavacca, F., Petrini, L., Massarotti, P., Schievano, S., Auricchio, F., Dubini, G., 2004. Stainless and shape memory alloy coronary stents: a computational study on the interaction with the vascular wall. Biomechanics and Modelling in Mechanobiology 2, 205–217.

Migliavacca, F., Petrini, L., Montanari, V., Quagliana, I., Auricchio, F., Dubini, G., 2005. A predictive study of the mechanical behaviour of coronary stents by computer modelling. Medical Engineering and Physics 27, 13–18.

Migliavacca, F., Gervaso, F., Prosi, M., Zunino, P., Minisini, S., Formaggia, L., Dubini, G., 2007. Expansion and drug elution model of a coronary stent. Computer Methods in Biomechanics and Biomedical Engineering 10, 63–73.

Morton, A.C., Crossman, D., Gunn, J., 2004. The influence of physical stent parameters upon restenosis. Pathologie-Biologie 52, 196–205.

Oh, S., Kleinberger, M., McElhaney, J.H., 1994. Finite-element analysis of balloon angioplasty. Medical and Biological Engineering and Computing 32, S108–S114.

Prendergast, P.J., Lally, C., Daly, S., Reid, A.J., Lee, T.C., Quinn, D., Dolan, F., 2003. Analysis of prolapse in cardiovascular stents: a constitutive equation for vascular tissue and finite-element modelling. Journal of Biomechanical Engineering 125, 692–699.

Raamachandran, J., Jayavenkateshwaran, K., 2007. Modeling of stents exhibiting negative Poisson's ratio effect. Computer Methods in Biomechanics and Biomedical Engineering 10, 245–255.

Rogers, C., Edelman, E.R., 1995. Endovascular stent design dictates experimental restenosis and thrombosis. Circulation 91, 2995–3001.

Rogers, C., Tseng, D.Y., Squire, J.C., Edelman, E.R., 1999. Balloon–artery interactions during stent placement: a finite element analysis approach to pressure, compliance, and stent design as contributors to vascular injury. Circulation Research 84, 378–383.

Schwartz, R.S., Huber, K.C., Murphy, J.G., Edwards, W.D., Camrud, A.R., Vlietstra, R.E., Holmes, D.R., 1992. Restenosis and the proportional neointimal response to coronary artery injury: results in a porcine model. The American Journal of Cardiology 19, 267–274.

Serruys, P.W., Kukreja, N., 2006. Late stent thrombosis in drug-eluting stents: return of the 'VB syndrome'. Nature Clinical Practice Cardiovascular Medicine 3, 637.

Serruys, P.W., van Der Giessen, W., Garcia, E., Macaca, C., Colombo, A., Rutsch, W., Vrints, C., Bonnier, H., Mudra, H., Fleck, E., Ormiston, J., Figulla, H., Seabra-Gomes, R., Veldhof, S., Morel, M.A., 1998. Clinical and angiographic results with the multi-link stent implanted under intravascular ultrasound guidance (West-2 study). Journal of Invasive Cardiology 10, 20B–27B.

Takashima, K., Kitou, T., Mori, K., Ikeuchi, K., 2007. Simulation and experimental observation of contact conditions between stents and artery models. Medical Engineering and Physics 29, 326–335.

Wang, W.Q., Liang, D.K., Yang, D.Z., Qi, M., 2006. Analysis of the transient expansion behavior and design optimization of coronary stents by finite element method. Journal of Biomechanics 39, 21–32.

Wentzel, J.J., Krams, R., Schuurbiers, J.C., Oomen, J.A., Kloet, J., van Der Giessen, W.J., Serruys, P.W., Slager, C.J., 2001. Relationship between neointimal thickness and shear stress after wall stent implantation in human coronary arteries. Circulation 103, 1740–1745.

Wu, W., Wang, W.Q., Yang, D.Z., Qi, M., 2007. Stent expansion in curved vessel and their interactions: a finite element analysis. Journal of Biomechanics 40, 2580.